Bull. Mater. Sci., Vol. 25, No. 2, April 2002, pp. 85–93. © Indian Academy of Sciences.

Photoelectronic properties of HgI_2 crystals for nuclear radiation detection

S L SHARMA* and H N ACHARYA

Department of Physics and Meteorology, Indian Institute of Technology, Kharagpur 721 302, India

MS received 2 June 2001; revised 2 February 2002

Abstract. Photoelectronic properties of red mercuric iodide single crystals, grown from its saturated solution in tetrahydrofuran, have been studied for the wavelength range 450–700 nm at temperatures 80, 110, 175, 235 and 300 K. Various aspects of the optical generation of charge carriers have been discussed. The computer simulation of the room temperature photoconductivity has generated the optimized values of the mobility–lifetime products ($\mu_e\tau_e = 5{\cdot}67 \times 10^{-5}$ cm^2/V, $\mu_h\tau_h = 0{\cdot}18 \times 10^{-5}$ cm^2/V), and surface recombination velocities ($S_e = 3{\cdot}2 \times 10^5$ cm/s, $S_h = 4{\cdot}5 \times 10^5$ cm/s) of the charge carriers in these crystals. The estimated values of the electron and hole drift lengths for typical electric fields suggest that, under the negative electrode illumination, THF α-HgI_2 crystals have high potential as regards to their use as photodetectors in most of the scintillation spectrometers.

Keywords. Mercuric iodide; photoconductivity; semiconductor detector; nuclear radiation detector.

1. Introduction

Red mercuric iodide (α-HgI_2) is a wide band gap semiconductor material ($E_g = 2{\cdot}13$ eV at 300 K) having exceptionally high atomic number (80·53). Due to the exceptionally low leakage current at room temperature and the higher absorption coefficients for X-rays and γ-rays, it was considered to be one of the most promising semiconductor materials for room temperature X-ray and γ-ray detection (Armantrout *et al* 1977). This led to the extensive studies on the material processing, crystal growth, detector fabrication and X-ray and γ-ray detection properties of this material (Lamonds 1983). Recently, α-HgI_2 single crystals have been used as photodetectors in scintillation spectrometers based on NaI(Tl), CsI(Tl), $CaWO_4$ and BGO scintillating materials (Iwanczyk *et al* 1983a,b, 1984; Markakis *et al* 1985). This has been so because these scintillating materials have their maximum light emission in the wavelength region 400–700 nm, which is the region of the highest photosensitivity for α-HgI_2 single crystals. In this technique of spectroscopy, the generation of charge carriers in α-HgI_2 single crystals solely depends upon the light emission of the scintillating material. In order to understand and fully exploit the potential of α-HgI_2 photodetector based scintillation spectrometers, it is highly desired to study photoresponse of α-HgI_2 single crystals grown by different growth techniques.

Till date, photocurrents for solution grown as well as for vapour phase grown α-HgI_2 single crystals were studied in order to determine the band gap energy, the temperature variation of the band gap energy (Bube 1957), the carrier trapping levels (Mohammed-Brahim *et al* 1983), the carrier lifetimes and the surface recombination velocities of the charge carriers (Burshtein *et al* 1986; Bornstein and Bube 1987). Burshtein *et al* (1986) studied the photoresponse of TOM crystals (the crystals grown by the temperature oscillation method) under the low-field as well as the high-field conditions. They explained their observations using Many's (1965) analysis, which assumes that, in the long wavelength region, the whole of the crystal is uniformly illuminated. This means that, in the long wavelength region, the photogeneration is uniform throughout the bulk of the crystal. This approximation holds only if the product of the absorption coefficient (α) and the crystal thickness (d) is much less than unity. As will be pointed out later that the value of the absorption coefficient for a good quality α-HgI_2 single crystal in the long wavelength region ($\lambda > 600$ nm) is about 25–30 cm^{-1}, above approximation does not hold for the crystal plates having thicknesses more than 50 μm. This may be the reason as to why the values of the electron and hole lifetimes reported by Burshtein *et al* (1986) greatly differ from the estimates of these parameters using X-ray excitations (Levi *et al* 1983a). Bornstein and Bube (1987) also studied the wavelength dependence of photoconductivity in TOM crystals in order to determine the diffusion lengths and lifetimes of electrons and holes. They analysed their measurements using De Vore's (1956) model which is

*Author for correspondence

applicable only under zero field conditions. For estimating the carrier lifetimes, they assumed constant values for the mobilities of electrons and holes.

The measurements on the photoelectronic properties of α-HgI_2 single crystals grown from solution based techniques are quite scanty. Moreover, there exists no measurement on the photoelectronic properties of α-HgI_2 single crystals grown from the saturated solution in tetrahydrofurane. As the photoelectronic properties help in determining the nuclear radiation detection grade of a photodetector for scintillation spectrometer, a detailed study was undertaken on the photoelectronic properties of α-HgI_2 single crystals grown in our laboratory from the saturated solution of α-HgI_2 in tetrahydrofurane. This study includes measurements on the wavelength dependence of photoconductivity at different temperatures in the temperature range 80–300 K and measurements on the thermally simulated currents. The measurements on thermally simulated currents were made in order to understand the temperature dependence of the photoconductivity in terms of the ionization of filled-traps in the different wavelength regions.

Further, we have developed an algorithm for simulating the photoconductivity vs wavelength spectrum (i.e. photoresponse). Using this algorithm, we simulated the room temperature photoresponse and obtained the optimized values of the transport properties (i.e. the electron mobility–lifetime product ($\mu_e\tau_e$), hole mobility–lifetime product ($\mu_h\tau_h$), electron surface recombination velocity (S_e) and hole surface recombination velocity (S_h), etc.) at room temperature.

2. Theoretical background

Consider a photodetector in the form of a large thin slab of thickness, d (see figure 1), whose one face is being illuminated by normally incident optical radiation of intensity, I_0 (photons/cm^2·s). According to the nature of the light absorption in a photodetector, we usually have a weak absorption region (photon energy, $h\nu < E_g$) and a strong absorption region ($h\nu \geq E_g$).

For the weak absorption region, the photons have long penetration depths inside the photodetector and hence the generation of electron–hole pairs can be assumed to take place throughout the bulk of the photodetector. If the thickness of the photodetector is such that the product αd (α being the absorption coefficient) is much greater than unity for all wavelengths under study, then the effect of multiple reflections from the two (parallel) faces can be neglected. As has already been pointed out that this is the case for α-HgI_2 photodetectors of thickness more than 50 μm. Therefore, the light intensity, I, at a distance, x, from the illuminated face can be expressed as

$$I = I_0 e^{-\alpha x}. \tag{1}$$

The corresponding rate of optical generation of electron–hole pairs per unit volume around a point at a distance, x, from the illuminated surface can be written as

$$G = \beta\alpha I = \beta\alpha I_0 e^{-\alpha x}, \tag{2}$$

where β denotes the photon quantum efficiency for electron–hole pair generation.

For parallel plate electrode geometry, under the high uniform electric fields within the photodetector, the diffusion current will be negligibly small as compared to the drift current. Therefore, the net carrier density $n(x)$ at a distance, x, from the illuminated electrode can be expressed as

$$\frac{dn}{dt} = G - \frac{n}{\tau}, \tag{3}$$

where τ denotes the effective lifetime of the charge carriers.

The solution of the above equation is

$$n(x) = G\tau[1 - e^{-t/\tau}] = \beta\alpha I_0 \tau e^{-\alpha x}[1 - e^{-t/\tau}]. \tag{4}$$

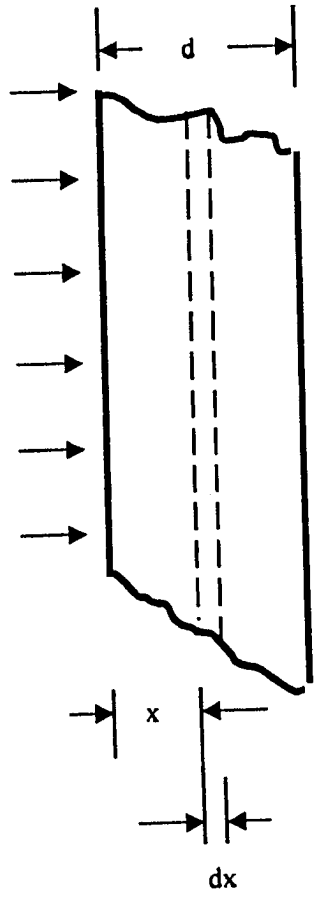

Figure 1. The sample geometry.

Now, for the negative electrode illumination, the electron and hole current densities can respectively be written as

$$J_e^{(-)} = \left(\frac{1}{d}\right)\int_0^d q\mu_e E n(x)\,dx,$$

$$= \left(\frac{qd_e\beta\alpha I_0}{d}\right)\int_0^d e^{-\alpha x}\left[1 - e^{-\frac{d-x}{d_e}}\right]dx,$$

$$= \left(\frac{qd_e\beta\alpha I_0}{d}\right)\left[\left\{\frac{1-e^{-\alpha d}}{\alpha}\right\} + \left\{\frac{e^{-\frac{d}{d_e}}(e^{-d[\alpha-(1/d_e)]}-1)}{[\alpha+(1/d_e)]}\right\}\right], \tag{5}$$

$$J_h^{(-)} = \left(\frac{qd_h\beta\alpha I_0}{d}\right)\left[\left\{\frac{1-e^{-\alpha d}}{\alpha}\right\} + \left\{\frac{(e^{-d[\alpha+(1/d_h)]}-1)}{[\alpha+(1/d_h)]}\right\}\right], \tag{6}$$

where q is the electronic charge, E the uniform electrostatic field inside the photodetector, d_e $(= \mu_e\tau_e E)$ the electron drift length, d_h $(= \mu_h\tau_h E)$ the hole drift length, μ_e the electron mobility, μ_h the hole mobility, τ_e the electron lifetime and τ_h the hole lifetime.

Thus, under the negative electrode illumination, the total current density is given by

$$J^{(-)} = J_e^{(-)} + J_h^{(-)},$$

$$= \left(\frac{q\beta\alpha I_0}{d}\right)\left[(d_e + d_h)\left\{\frac{1-e^{-\alpha d}}{\alpha}\right\}\right.$$

$$\left. + d_e\left\{e^{-d/d_e}\,\frac{e^{-d\left(\alpha-\frac{1}{d_h}\right)}-1}{\left(\alpha-\frac{1}{d_e}\right)}\right\} + d_h\left\{\frac{e^{-d\left(\alpha+\frac{1}{d_h}\right)}-1}{\alpha+\frac{1}{d_h}}\right\}\right]. \tag{7}$$

Similarly, under the positive electrode illumination, the total current density can be expressed as

$$J^{(+)} = J_e^{(+)} + J_h^{(+)},$$

$$= \left(\frac{q\beta\alpha I_0}{d}\right)\left[(d_e + d_h)\left\{\frac{1-e^{-\alpha d}}{\alpha}\right\}\right.$$

$$+ d_e\left\{e^{-\frac{d}{d_e}}\left\{\frac{e^{-d\left(\alpha+\frac{1}{d_e}\right)}-1}{\alpha+\frac{1}{d_e}}\right\}\right\}$$

$$\left. + d_h\left\{\left\{e^{-d/d_h}\,\frac{(e^{-d[\alpha-(1/d_h)]}-1)}{\left(\alpha-\frac{1}{d_h}\right)}\right\}\right\}\right]. \tag{8}$$

For the photon energy, $h\nu \geq E_g$, the light is absorbed within a very thin layer of the photodetector in comparison to its thickness, d (i.e. the light penetration depths are much smaller than the thickness of the photodetector). The generation of the electron–hole pairs can then be assumed to be zero everywhere in the bulk of the photodetector except at the illuminated surface, where the generation rate per unit area is $G_s = \beta I_0$. So, under the negative electrode illumination only electrons and under the positive electrode illumination only holes are injected into the bulk of the medium. Therefore, under the negative electrode illumination, we can write

$$G_s = [\mu_e E + S_e]n_e(0), \tag{9}$$

where $n_e(0)$ is the surface electron density and S_e denotes the rate of surface recombination for each electron (i.e. the electron surface recombination velocity). The first term on the right side of the above equation represents the particle current leaving the surface and the second term represents the rate of surface recombination. From (9), we get

$$n_e(0) = \frac{\beta I_0}{\mu_e E + S_e}. \tag{10}$$

So, the electron density at any point at a distance, x, from the illuminated surface can be written as

$$n_e(x) = \left(\frac{\beta I_0}{\mu_e E + S_e}\right)e^{-\frac{x}{d_e}}. \tag{11}$$

Thus, the photocurrent density under the negative electrode illumination becomes

$$J_S^{(-)} = \left\{\frac{q\beta I_0}{[\mu_e E + S_e]}\right\}\left\{\frac{\mu_e E}{d}\right\}\int_0^d e^{-x/d_e}\,dx,$$

$$= \left\{\frac{q\beta I_0}{[1+(S_e/\mu_e E)]}\right\}\left\{\frac{d_e}{d}\right\}\left[1-e^{-d/d_e}\right]. \quad (12)$$

Similarly, under the positive electrode illumination, the photocurrent density can be written as

$$J_S^{(+)} = \left\{\frac{q\beta I_0}{[1+(S_h/\mu_h E)]}\right\}\left\{\frac{d_h}{d}\right\}\left[1-e^{-d/d_h}\right], \quad (13)$$

where S_h denotes the rate of surface recombination for each hole (i.e. the hole surface recombination velocity).

3. Experimental

Commercially available α-HgI_2 contains traces of metallic impurities which can be removed by repeated sublimation (Lamonds 1983). In the present study, E–MERCK α-HgI_2 powder (98% assay) was purified by six-time sublimation followed by two-time crystallization from dimethylsulfoxide–methylalcohol–α-HgI_2 (DMSO–MeOH–α-HgI_2) saturated solution.

Tetrahydrofurane (THF) is a potential aprotic organic solvent for α-HgI_2. Bohac (1983), for the first time, grew large single crystals of α-HgI_2 by isothermal solvent evaporation from its saturated solution in THF. At 20°C, the saturated solution has a density of 1·5 g/cm^3 which goes up to 1·55 g/cm^3 for supersaturated solution. A broad metastable Ostwald–Miers region allows rapid crystal growth.

A saturated solution of purified α-HgI_2 was prepared in THF. Subsequently, the solution was filtered into a clean beaker and was covered with a few layers of filter paper having a few holes to control the rate of solvent evaporation. The beaker was then placed in a constant temperature water-bath maintained at 25°C. The time taken for complete solvent evaporation from a 100 ml solution was about ten days. Crystals weighing up to 14 g could thus be grown. A remarkable improvement was observed when a small amount of iodine (99·9% pure) was added into the saturated solution. Larger single crystals weighing as large as 31 g could thus be grown. As the purified material is expected to be non-stoichiometric and mercury-rich, addition of iodine into the solution compensates the iodine-deficiency and improves the size of the single crystals. On complete solvent evaporation, crystals of various shapes and varied orientations were found at the bottom of the beaker. Large crystals have surface dislocations and are not fully transparent throughout the bulk. Smaller crystals, however, have no visible surface dislocations and fully transparent throughout the bulk. For photoelectronic characterization, samples of sizes about 5 × 5 × 1 mm^3 were cleaved perpendicular to the c-axis from large crystals obtained after adding small amount of iodine in the solution. A few of the cleaved samples were etched in 10% aqueous KI solution for about 10 min. Electrical contacts were made by painting thin layer of aquadag on the opposite faces of each of the samples.

For recording a photoconductivity spectrum each time, a sample was mounted inside a cryostat. An electric field of about 2 × 10^3 V/cm was applied parallel to the c-axis of the crystal. After cooling the crystal to a desired temperature, the steady state photocurrents were recorded at different wavelengths in the range of wavelengths 450–700 nm. The interval of wavelengths was chosen to be about 10 nm. The photoconductivity spectra were recorded at temperatures 80, 110, 175, 235, and 300 K for several unetched and etched samples under negative as well as positive electrode illumination. The beam of monochromatic light was obtained from an ORIEL lamp-monochromator assembly (Model Nos 7340 and 77250, respectively). Photocurrents were measured with a KEITHLEY 610C Electrometer Amplifier. The photoconductivity spectra were subsequently analysed in the light of the theory outlined in §2.

For the measurements on the thermally stimulated currents (TSC), the sample under investigation was excited at liquid nitrogen temperature by means of photons of energy equal to the band gap energy at liquid nitrogen temperature. After filling the traps, the excitation was stopped and the sample was then heated in dark to 300 K at a constant heating rate of about 0·2 K/s. The temperature of the sample was monitored by measuring emf of a copper-constantan thermocouple placed close to the sample. Accuracy of the temperature measurements was ± 1 K. The current in excess to the dark current, resulting due to the release of the trapped charge carriers into the valence band (for holes) or conduction band (for electrons), was monitored by the KEITHLEY 610C Electrometer Amplifier as a function of the temperature of the sample and was recorded on a X–Y recorder. In this manner, TSC spectra were recorded for several samples. Different peaks in a TSC spectrum represent different trapping levels. The TSC spectra were analysed using the method of Pal *et al* (1995).

4. Results and discussion

Figure 2 shows a typical optical absorption for α-HgI_2 single crystals grown by isothermal solvent evaporation from the saturated solution of α-HgI_2 in THF (henceforth these crystals will be referred to as THF crystals). The optical absorption spectrum was recorded at room temperature (~ 300 K). Clearly, the lowest value of the absorption coefficient (α) is about 30 cm^{-1} in the wavelength region 600–700 nm. From the absorption edge, the estimate of the band gap energy (E_g) is found to be 2·12 ± 0·01 eV, a value matching reasonably well with the reported values (Burger and Nason 1992).

Figure 3 shows the typical TSC spectra for three good quality THF crystals. It is seen that these crystals, in

general, possess four peaks at 135 K, 170 K, 195 K, 210 K and an intense peak at 275 K. Table 1 lists these temperatures along with the corresponding activation energies.

Figure 4 shows the typical photoconductivity spectra for the etched samples at different temperatures under negative as well as positive electrode illumination. Similar spectra for the unetched samples are shown in figure 5. Each of these spectra was obtained by normalizing different regions of a recorded photoconductivity spectrum with respect to the photon flux of 5×10^{14} photons/$cm^2 \cdot s$ at $\lambda = 580$ nm. The photoconductivity under negative electrode illumination is always higher than that under positive electrode illumination. This is quite similar to the observation of Bornstein and Bube (1987) but is in contradiction with what Burshtein *et al* (1986) has reported. Surprisingly enough, both these groups performed their studies on the crystals grown by temperature oscillation method. The difference in the two photoconductivities, observed in the present study, indicates that the drift length for electrons is much higher than that for holes.

In order to understand the shapes of the photoconductivity spectra, each of these spectra can be divided into three spectral regions:

- The wavelength range 700–590 nm corresponds to the weak absorption region where the photoconductivity increases rapidly on lowering the wavelength.
- The wavelength range 590–550 nm corresponds to the transition region where each of the photoconductivity spectra possesses a sharp peak.
- The wavelength range 550–450 nm corresponds to the strong absorption region where the photoconductivity decreases rather slowly on lowering the wavelength and shows more or less a plateau behaviour.

For the weak absorption region (700 nm ≥ wavelength ≥ 590 nm), assuming uniform carrier generation throughout the bulk of the crystal, the photoconductivity spectra under negative and positive electrode illumination are expected to be identical. Experimentally, however, the photoconductivity under negative electrode illumination is higher. This is so because the carrier generation is not uniform throughout the bulk of the crystal. As the product 'αd' is greater than unity for typical electrode separations of about 400 μm, the carrier generation is more near the illuminated electrode and decreases quite appreciably along the thickness of the crystal. Though the total photocurrent comprises of the contribution from the bulk as well as from the surface, a direct calculation using (6), (7), (12) and (13) for the present case shows that the surface contribution in this region is negligible as compared to the bulk contribution (i.e. $J_s^{(-)}/J^{(-)}$ and $J_s^{(+)}/J^{(+)} \sim 10^{-3}$). This shows that the increase in the photoconductivity under negative electrode illumination is due to an increase in the overall charge collection efficiency.

Further, in the weak absorption region, a photoconductivity spectrum is expected to be similar to the corresponding absorption spectrum. Due to a large increase in the quantum efficiency (β) with the energy of the

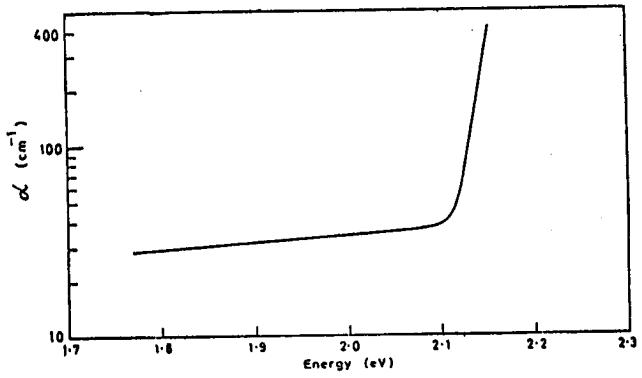

Figure 2. Typical absorption spectrum for THF α-HgI_2 crystals.

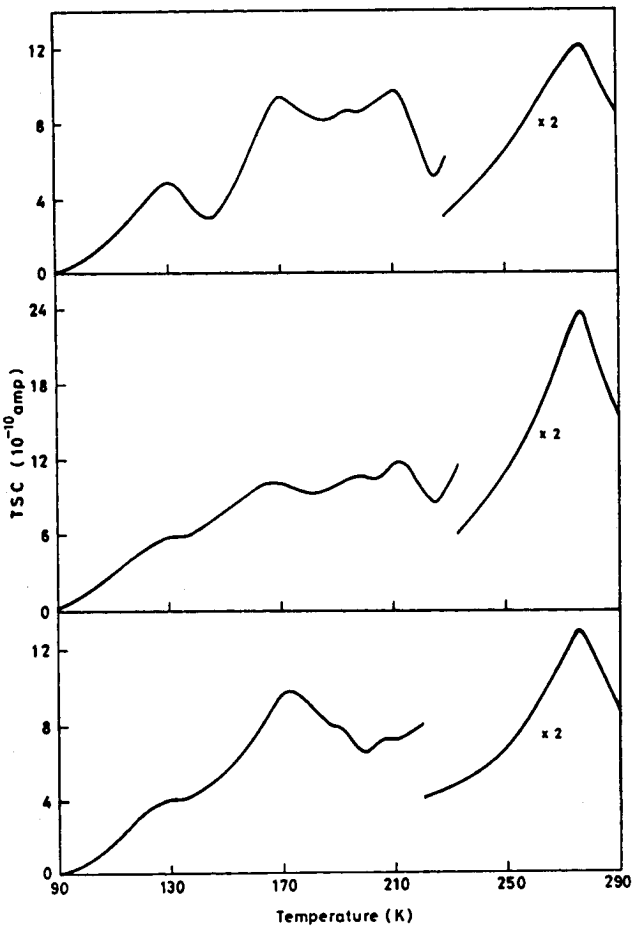

Figure 3. TSC spectra for three good quality THF α-HgI_2 crystals.

incident light, however, the former shows a sharp rise. The photoconductivity spectra recorded at low temperatures show a shoulder at about 6200 Å. This is similar to what Bube (1957), Hyder (1977) and Burshtein *et al* (1986) observed. Bube (1957) and Hyder (1977) also observed a photoluminescence peak at around 6200 Å in their crystals. Merz *et al* (1983) noticed the disappearance of the photoluminescence peak at about 6200 Å upon purification. Recent studies on photoluminescence of α-HgI_2 single crystals (James *et al* 1992), however, confirmed the appearance of the band at around 6200 Å in all the detector grade crystals with different relative intensities and slightly different energies. This band, previously thought to be due to impurities, showed no change in several doping experiments. The shoulder at about 6200 Å, observed in the low temperature photoconductivity spectra, has been confirmed by Lopez-Cruz (1989) to be due to the indirect band gap in α-HgI_2 at about 2 eV. The absence of this shoulder in the photoconductivity spectra, recorded at higher temperatures, may be due to the shift of peaks of the photoconductivity spectra towards longer wavelength side at higher temperatures.

Around the peak region of the photoconductivity spectra, the absorption coefficient (α) rises very rapidly from about 30 cm^{-1} to about 200 cm^{-1} as well as the quantum efficiency attains its maximum value. Thus, the charge carrier generation close to the illuminated electrode is many orders of magnitude higher than that near the other electrodes. The pronounced difference between the photoconductivity spectra for negative and positive electrode illumination, therefore, can be attributed to the large mobility–lifetime product ($\mu\tau$) for electrons as compared to that for holes. Another difference can be noted in the spectra at all temperatures that the peak position under positive electrode illumination occurs at a slightly higher wavelength. The onset of the surface recombination of holes at a higher wavelength than that of electrons may be responsible for this difference. In the peak region, higher photocurrents for etched samples as compared to that for unetched crystals (refer to figures 4 and 5) can be understood in terms of the higher surface recombinations in the case of unetched samples. On etching, some of the surface defects are removed resulting into lower values of surface recombination velocities. It is also observed that the peak photocurrent has a maximum at around 170 K (see figure 6). This may be due to the thermal ionization of the slow retrapping type electron trapping centres (Schlesinger *et al* 1992; Pal *et al* 1995) at 0·31 eV, which releases trapped charge carriers and thereby increase the overall photoconductivity. From values of the peak wavelength, the values of band gap energy (E_g) at different temperatures were calculated using the relationship: E_g (in eV) = 1·24/λ (in μm). Figure 7 shows the dependence of the band gap energy on temperature. This dependence is more or less linear, except at low temperatures. The temperature coefficient of the band gap energy was determined from the linear

Table 1. Activation energies of different trapping levels in THF crystals.

TSC peak temperature, T_m (K)	Activation energy (eV)
135	0·15
170	0·31
195	0·44
210	0·50
275	0·70

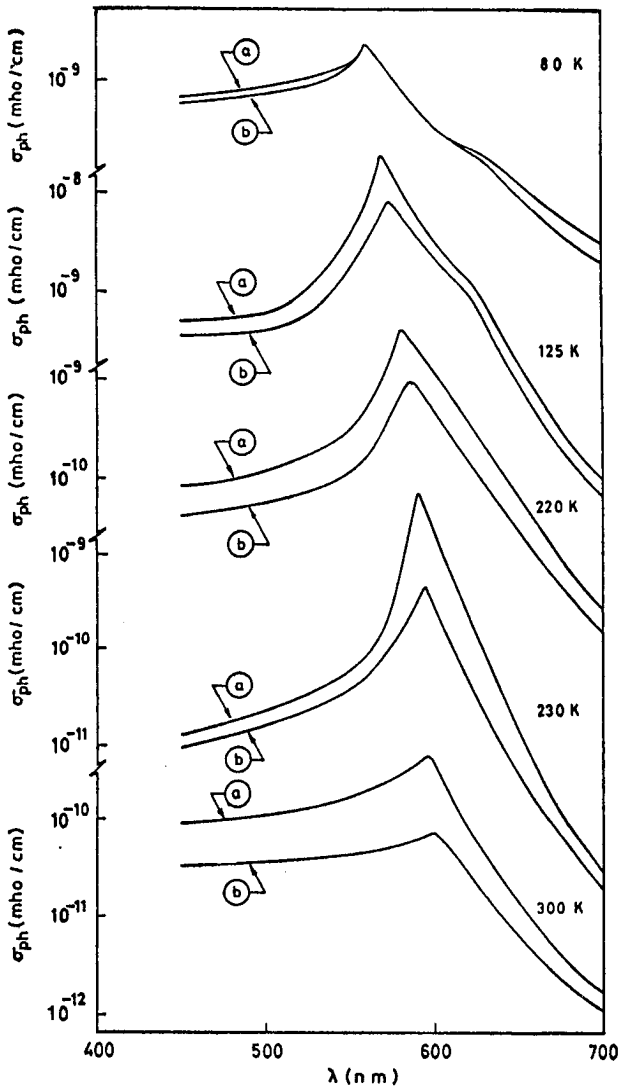

Figure 4. Typical photoconductivity spectra for etched samples at different temperatures: (a) under the negative electrode illumination and (b) under the positive electrode illumination.

part of the curve and was found to be about $(-4{\cdot}1 \times 10^{-4})$ eV/K, a value which matched reasonably well with the reported values (Burger and Nason 1992).

In the slowly varying region of the photoconductivity spectra, the light is totally absorbed within a very small thickness (i.e. within a few micrometres) of the sample close to the illuminated surface. This gives rise to the photoconductivity strongly dominated by the surface and near-surface contributions. Therefore, the photocurrent under negative electrode illumination is solely due to electrons and that under positive electrode illumination is solely due to holes. It was observed that the change in the photoconductivity under the positive electrode illumination is quite small as compared to that under the negative electrode illumination on lowering the wavelength from 550 nm to 450 nm. This may be due to two different reasons: (i) the surface recombination velocity for electrons may be increasing with photon energy and (ii) the density of the electron recombination centres may be nonuniform in the surface region and is maximum at the top of the illuminated surface. The photon energy

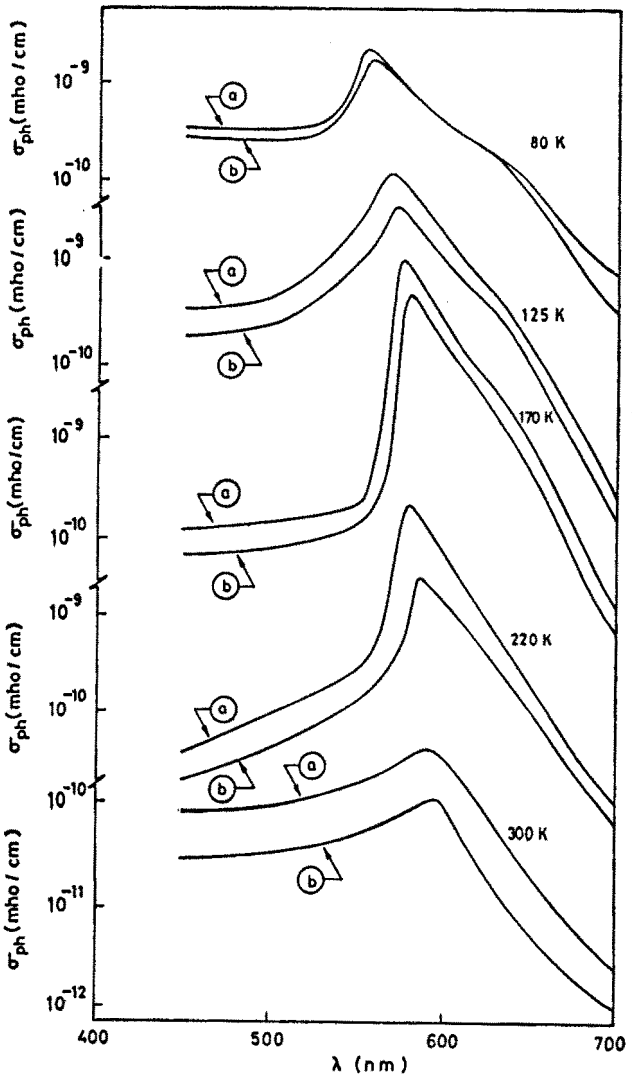

Figure 5. Typical photoconductivity spectra for unetched samples at different temperatures: (a) under the negative electrode illumination and (b) under the positive electrode illumination.

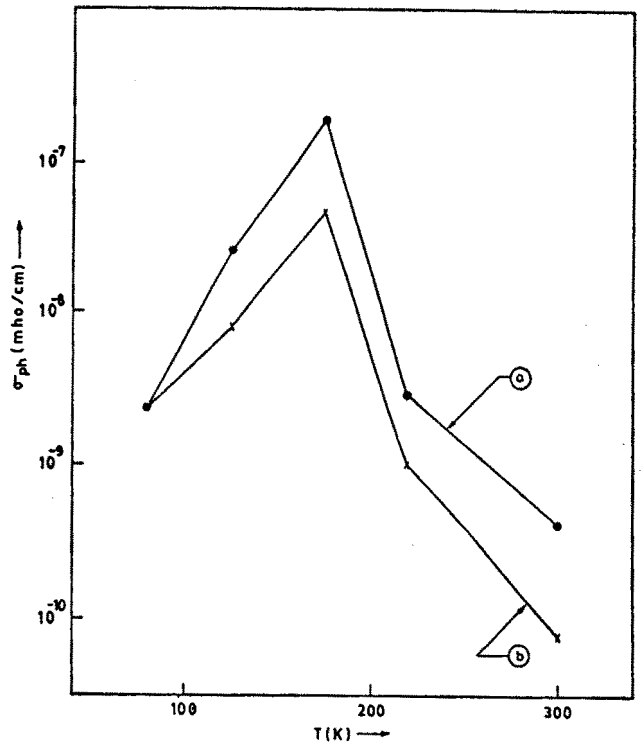

Figure 6. Temperature dependence of the peak photocurrent: (a) under the negative electrode illumination and (b) under the positive electrode illumination.

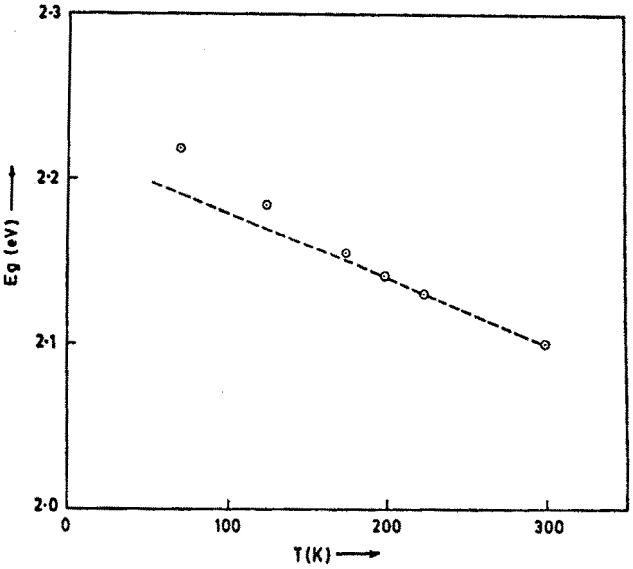

Figure 7. Variation of the band gap energy (E_g) of α-HgI_2 crystals with temperature.

dependence of the electron surface recombination velocity was also reported by Burshtein *et al* (1986).

In order to determine the charge carrier transport properties in THF crystals, the room temperature photoconductivity spectra for the etched and unetched samples were theoretically simulated. For the theoretical simulation of a photoconductivity spectrum, we have used the presently determined absorption coefficients and quantum efficiencies for different wavelengths, $\mu_e = 100$ cm^2/V·s, $\mu_h = 15$ cm^2/V·s, $\tau_e = 4$ μs, $\tau_h = 0{\cdot}75$ μs, and $S_e = S_h = 10^5$ cm/s. The surface recombination thickness was assumed to be about 5 μm. The values of other parameters were set according to the present experimental conditions. The quantum efficiency at a wavelength was evaluated from the photocurrent at that wavelength under negative electrode illumination in a sample of thickness of about 40 μm. As the quantities 'αd' and 'd/d_e' are both much smaller as compared to unity for the sample of thickness of about 40 μm, the corresponding photocurrent density under negative electrode illumination can be expressed as

$$J^{(-)} = q\beta\alpha I_0 d. \tag{14}$$

Thus, the corresponding quantum efficiency can be evaluated from the relationship:

$$\beta = \frac{J^{(-)}}{q\alpha I_0 d}. \tag{15}$$

The wavelength dependence of the quantum efficiency for the THF crystals, so obtained, is shown in figure 8. The mobility–lifetime products ($\mu_e\tau_e$, $\mu_h\tau_h$) of the charge carriers were first optimized such that the simulated spectrum matched reasonably well with the experimental spectrum in the weak absorption region (590 nm < λ < 700 nm). This is quite reasonable because, in this region, the surface contribution to the total photocurrent is negligibly small. Using the optimized values of the mobility–lifetime products, once again, the total photoconductivity spectrum was generated. It was seen that the simulated spectrum deviated from the experimental spectrum only in the strong absorption region (450 nm < λ < 550 nm). Subsequently, the values of the surface recombination velocities (S_e, S_h) were optimized in order to match the simulated spectrum with the experimental spectrum in the strong absorption region where the bulk contribution is negligibly small compared to the surface contribution. Cutting samples from a large single crystal of a soft material, like α-HgI_2, produces a large number of surface defects which may act as electron and hole trapping

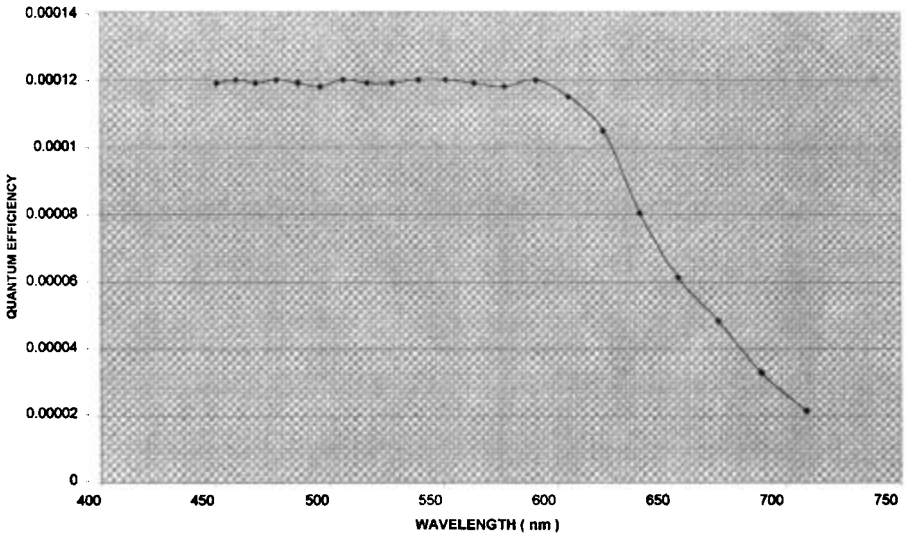

Figure 8. Variation of the quantum efficiency (β) for α-HgI_2 crystals with wavelength of the incident light.

Table 2. Optimized transport properties of charge carriers.

Property	Value for unetched sample	Value for etched sample
Electron mobility–lifetime product ($\mu_e\tau_e$)	$4{\cdot}62 \times 10^{-5}$ cm^2/V	$5{\cdot}67 \times 10^{-5}$ cm^2/V
Hole mobility–lifetime product ($\mu_h\tau_h$)	$0{\cdot}05 \times 10^{-5}$ cm^2/V	$0{\cdot}18 \times 10^{-5}$ cm^2/V
Electron surface recombination velocity (S_e)	$2{\cdot}2 \times 10^6$ cm/s	$3{\cdot}2 \times 10^5$ cm/s
Hole surface recombination velocity (S_h)	$7{\cdot}0 \times 10^5$ cm/s	$4{\cdot}5 \times 10^5$ cm/s

centres. Etching removes a large fraction of these defects and improves the transport properties. A large improvement in the hole mobility–lifetime product ($\mu_h\tau_h$) suggests that the majority of the surface defects in the unetched samples act as hole trapping centres. Table 2 lists the optimized values of all the transport parameters. Except the value of S_e, the values of all other parameters for etched samples match fairly well with those values reported previously for nuclear radiation detector quality crystals (Levi *et al* 1983b). The value of the surface recombination velocity for electrons (S_e) is almost an order of magnitude higher than the value reported by Levi *et al* (1983a,b). Though surface conditions improve on etching, however, the same are not optimal as regards to the electron surface recombination. For the electric field strength of about 2×10^3 V/cm, the estimated values of the electron and hole drift lengths are 1150 μm and 50 μm, respectively. The typical thickness of α-HgI_2 photodetector for any scintillation spectrometer is about 300 μm. So, under the negative electrode illumination, THF α-HgI_2 crystals present high potential for their use as photodetectors in conjunction with most of the scintillation spectrometers.

5. Conclusions

All the photoconductivity spectra show a sharp rise on lowering the wavelength from 700 nm to 600 nm which corresponds to the weak absorption region, pass through a maximum within the wavelength range 600–550 nm and finally go to a slowly varying region below 550 nm which corresponds to the strong absorption region. Analysis shows that the photoconductivity in the weak absorption region is solely governed by the bulk processes while that in the strong absorption region is totally controlled by the generation and recombination of charge carriers on and near the surface. The magnitude of the peak photoconductivity goes through a maximum at around 170 K. This maximum may be associated with the slow retrapping type electron traps at 0·31 eV which get thermally ionized around this temperature and contribute to the overall photoconductivity. From the temperature dependence of the peak wavelength, the temperature coefficient of the band gap was found to be about $(-4{\cdot}1 \times 10^{-4})$ eV/K. Computer simulation of the room temperature photoconductivity spectra for etched samples allowed us to determine the optimized values of mobility–lifetime products and surface recombination velocities for electrons and holes in THF crystals. The estimates of the drift lengths for the two charge carriers suggest that, under the negative electrode illumination, THF α-HgI_2 crystals can be successfully used as photodetectors in most of the scintillation spectrometers. Further work is in progress (a) to simulate the photoconductivity spectra recorded at other temperatures and determine temperature dependences of different transport properties and (b) to study the performance of a THF α-HgI_2 photodetector based scintillation spectrometer.

References

Armantrout G A, Swierkowski S P, Sheroman J W and Yee J H 1977 *IEEE Trans. Nucl. Sci.* **NS-24** 121

Bohac P 1983 *J. Cryst. Growth* **61** 163

Bornstein J and Bube R H 1987 *J. Appl. Phys.* **61** 2676

Bube R H 1957 *Phys. Rev.* **106** 703

Burger A and Nason D 1992 *J. Appl. Phys.* **71** 2717

Burshtein Z, Akujieze J K and Silberman E 1986 *J. Appl. Phys.* **60** 3182

De Vore H B 1956 *Phys. Rev.* **102** 86

Hyder S B 1977 *J. Appl. Phys.* **48** 313

Iwanczyk J S *et al* 1983a *Nucl. Instrum. Meth.* **213** 123

Iwanczyk J S, Barton J V, Dabrowski A J, Kusmiss J H and Szymczyk W M 1983b *IEEE Trans. Nucl. Sci.* **NS-30** 363

Iwanczyk J S, Dabrowski A J, Markakis J, Ortale C and Schnepple W F 1984 *IEEE Trans. Nucl. Sci.* **NS-31** 336

James R B, Bao X J, Schlesinger T E, Cheng A Y, Ortale C and Van den Berg L 1992 *Nucl. Instrum. Meth. Phys. Res.* **A322** 435

Lamonds H A 1983 *Nucl. Instrum. Meth.* **213** 5

Levi A, Burger A, Schieber M M, Van den Berg L, Yelton W B and Alkire R W 1983a *Nucl. Instrum. Meth.* **213** 31

Levi A, Schieber M M and Burshtein Z 1983b *J. Appl. Phys.* **54** 2472

Lopez-Cruz E 1989 *J. Appl. Phys.* **65** 874

Many A 1965 *J. Phys. Chem. Solids* **26** 575

Markakis J, Ortale C, Schnepple W F, Iwanczyk J S and Dabrowski A J 1985 *IEEE Trans. Nucl. Sci.* **NS-32** 559

Merz J L, Wu Z L, Van den Berg L and Schnepple W F 1983 *Nucl. Instrum. Meth.* **213** 51

Momammed-Brahim T, Friant A and Mellet J 1983 *Phys. Status Solidi* **(a)79** 71

Pal T, Sharma S L and Acharya H N 1995 *J. Phys. D: Appl. Phys.* **28** 1439

Schlesinger T E, Bao X J, James R B, Cheng A Y, Ortale C and Van den Berg L 1992 *Nucl. Instrum. Meth. Phys. Res.* **A322** 414